A Novel Approach for Modeling Bubbling Gas–Solid Fluidized Beds

Javier Villa Briongos, Sergio Sanchéz-Delgado, Antonio Acosta-Iborra, and Domingo Santana
Universidad Carlos III de Madrid, Escuela Politécnica Superior, Departamento de Ingeniería Térmica y de Fluidos, Avenida de la Universidad 30, 28911 Leganés, Madrid, Spain

DOI 10.1002/aic.12375
Published online August 26, 2010 in Wiley Online Library (wileyonlinelibrary.com).

A phenomenological discrete bubble model is proposed to help in the design and dynamic diagnosis of bubbling fluidized beds. An activation region mechanism is presented for bubble formation, making it possible to model large beds in a timely manner. The bubbles are modeled as spherical-cap discrete elements that rise through the emulsion phase that is considered as a continuum. The model accounts for the simultaneous interaction of neighboring bubbles by including the trailing effects due to the wake acceleration force. The coalescence process is not irreversible and therefore, the coalescing bubble pair is free to interact with other rising bubbles originating the splitting phenomena. To validate the model, the simulated dynamics are compared with both experimental and literature data. Time, frequency, and state space analysis are complementarily used with a multiresolution approach based on the empirical method of decomposition to explore the different dynamic scales appearing in both the simulated time series and those obtained from experimental runs. It is concluded that the bubble dynamics interactions play the main role as the driver of the resulting bed dynamics, matching the main features of measured bubble dynamics. Exploding bubble phenomena have been identified by establishing a direct relation between the bubble generation, interaction and eruption, and the measured signals. © 2010 American Institute of Chemical Engineers *AIChE J,* 57: 1733–1750, 2011
Keywords: fluidization, multiscale modeling, bubble phenomena, chaos, multiresolution analysis

Introduction

Among the huge number of industrial applications of bubbling gas–solid fluidized beds (FBs), those related to their use in energy conversion have recently gained attention due to the current energy policies. Thus, bubbling gas–solid FBs are broadly applied in thermochemical energy conversion processes such as combustion and gasification. The fluidization process offers a high heat transfer rate, good gas–solid mixing and solid handling, and provides a uniform and controllable temperature. Moreover, its ability to process low grade fuels with low pollutant emission makes the use of bubbling FBs a very promising technology for the necessary valorization of biomass and wastes in energy conversion processes.[1] However, for instance, when dealing with biomass FB processes, the high complexity characterizing conventional gas–solid FBs dynamics increases due to the limited research reported on biomass fluidization hydrodynamics. According to that, recently it has been pointed out the necessity of improving the characterization of biomass fluidization hydrodynamics to understand the influence of the biomass particles on the fluidization phenomena.[2]

The characterization of gas–solid FB dynamics is currently addressed by monitoring the local time evolution of some

This work is dedicated to the memory of Dr. Andrés Cabanillas (CIEMAT) who collaborated during the bench scale combustor measurements.

Correspondence concerning this article should be addressed to J. V. Briongos at jvilla@ing.uc3m.es.

variables such as pressure, capacitance, temperature, etc.[3] Moreover, some global techniques addressed to characterize the overall FB dynamics have been also reported.[4–7] Subsequently, to elucidate the dynamical processes occurring within the FB system, the time-dependent behavior of the measured signals is often analyzed by time and frequency domain analyses.[8] However, due to the inherent nonlinear features of gas–solid FB dynamics, a nonlinear approach including a multiscale analysis and tools derived from the deterministic chaos theory, can be reliably applied complementarily to the time and frequency analysis methods to account for those nonlinear interactions.[9] Thus, dynamical aspects characteristics of gas–solid fluidization are identified by establishing a direct relation between the physical phenomena driving the dynamics and the measured signals. Nevertheless, when dealing with complex processes such as the fluidization of biomass particles, previous literature often neglects critical dynamical aspects related to biomass particle properties, ash features, or endogenous bubble generation,[10] which makes even harder the understanding of the physical phenomena behind the measured signals. According to that, to improve the characterization of the dynamics of bubbling gas–solid FBs, it is requisite to understand both the dynamics behind the measured signals and the way the different signal properties obtained from the digital signal processing are related to the physical phenomena occurring within the FBs. Thus, CFD models of gas–solid systems are often used to extract information useful to guide design and operation of FBs.[11] During the last decade due to the shocking increase of the computer capabilities, there is a huge number of literature dealing with gas–solid FB modeling. The models can be divided into two main groups: Eulerian–Eulerian models that consider the gas and solid phases as interpenetrating continua,[12–14] and Eulerian–Lagrange models that coupling a Lagrangian description of the particle dynamics with a continuum description of the gas phase.[15]

Either the continuum or the discrete element method approaches involve a detailed description of the flow; in one hand, the discrete particle model (DPM) approach[16] try to describe the large-scale dynamics appearing in FBs by direct modeling of the particle–particle and gas–particle interactions. Although DPM is a very powerful tool to study the details of the multiscale flow structure characterizing gas–solid FBs, however, it is well known that the success of the DPM models is not guaranteed as a detailed description of particle dynamics is not always possible,[15] and some correlations between the small- and large-scale dynamics can be missed. Besides, the vast computational effort needed to model a large number of particles limits its use when modeling large FB units. On the other hand, the continuum approach, although it is also time consuming, can be used fairly well for scale-up design studies. However, the information provided on dynamic characteristics is very limited and its solution strongly depends on empirical closure relationships. Furthermore, to manage industrial size problems, it has been proposed the use of coarse grid models,[17] accounting the effects of smaller unresolved dynamical structures through the use of subgrid closures. More recently, Wang et al.[18] reported a coarse grid method where drag correlation obtained from homogeneous fluidization are modified to simulate the heterogeneous structure of a bubbling FB. However, as pointed out previously,[17] the main limitation of the coarse grid models lies on the subgrid scale structure. Thus, although the coarse grid approach is very promising, there is not a way to decide what grid size should be used for a given problem. Besides, the homogeneous or inhomogeneous features characterizing the subgrid scale structure will depend on the different bubble and solid circulation patterns characterizing the FB, which, in the end, can be formed depending on bed geometry, operating conditions, distributor design, etc. Moreover, it has been reported in literature the limitation of CFD models due to the imposed boundary conditions at the distributor level.[19] The fact that CFD models assume that gas enters the column distributed in a perfectly uniform manner and at constant pressure ignores gas feeding factors such as the gas supply system or the distributor plate, which can influence FB dynamics.[20]

Besides the limitation imposed by the modeling approach, few works in the literature validate the simulated behavior of the FB using the same information that is currently measured during FB monitoring such as pressure fluctuation signals.[21] Furthermore, due to the detailed description of FB dynamics, in the end both the continuum and the DPM approaches become as complex to characterize as the experimental unit, making it difficult to identify and therefore to establish a direct connection between the bed dynamics phenomena and the measured signals. To simplify the problem, some simpler models have been proposed in literature to diminish the number of variables by studying either the particle or the bubble dynamics,[22,23] to later extrapolate the information provided during the simulation to the observed experimental behavior. According to that, two recent different approaches addressed the discrete bubble modeling of FBs, DBM. They have shown to be useful for modeling global dynamics of large-scale FBs. Thus, the dynamic interacting bubble simulation (DIBS) model proposed by Pannala et al.[24] accounts for the simultaneous interactions of individual bubbles and have been successfully applied for reacting FBs. However, the fact that both the bubble rise velocity and the trailing effect between rising bubbles are based on empirical correlations make the general use of DIBS difficult for modeling bubbling FBs. In contrast to the DIBS model, the DBM reported by Bokkers et al.[25] fully accounts for the two-way coupling between the emulsion phase and the rising bubbles, which are considered as discrete spherical elements that rise according to the second law of motion. Moreover, the model reported by Bokkers et al.[25] includes the bubble–bubble and bubble–wall interaction to model the coalescence process. Nevertheless, the force resulting from bubble to bubble interaction due to wake effect is ignored, and the inclusion of the Eulerian solution for the dense phase increases the computational cost.

In this article, a DBM approach is presented to help the understanding of the dynamics behind the measured signals and consequently, to improve the existing monitoring methods by connecting the different signal parameters obtained from the time series analysis to the physical phenomena occurring within FBs. In contrast to previous discrete bubble models reported in literature, a wake acceleration force is proposed to account for the bubble trailing interaction. The force balance is based on the pressure recovery in the wake below a spherical cap bubble.[26]

Moreover, the proposed model takes into account the distributor performance by means of a novel activation region (AR) mechanism, which is proposed to explain the multiorifice bubble generation. It is shown that the bubble formation can follow a certain generation rate and injection pattern ruled by the probability of bubble formation over the different distributor regions. Furthermore, the bubbles are considered as discrete spherical caps and are tracked individually by integrating the equations derived from the second law of motion. The model uses a direct implementation of the bubble coalescence and does not make any prior assumption on bubble encounter frequency. As a result, the proposed DBM provide information to develop design strategies to manipulate macroscale flow structures, and to help identifying the characteristic length scales to be used in more sophisticated approaches such as coarse grid models, as well as information regarding bubble generation that can be used to improve existing CFD models by modifying the boundary conditions to be used.

The Discrete Bubble Model

Model basis

The proposed model is a discrete phenomenological approach where bubbles are modeled as spherical-cap discrete elements that rise through the emulsion phase, which is considered as a continuum. The modified two-phase theory, in which it is considered that not all the excess gas, $U_e = U_0 - U_{mf}$, passes through the bed as observable bubbles, is used to estimate the visual bubble flow. Accordingly, the visible bubble flow, V_b, is given by the well-known relationship:

$$V_b = \psi U_e A_{bed}$$

where ψ is the dimensionless ratio between the observed bubble flow and the excess flow from the two-phase theory,[27] and it is estimated according to the correlation proposed by Johnsson et al.[28] Furthermore, the bubbles are dynamically coupled to its closest leading neighbor through a wake acceleration force that accounts for the bubble trailing interaction. The bubble coalescence is modeled including a shrinking/growing mechanism that gradually increases or decreases the size of the coalescing bubble pair. Moreover, bubble formation at the distributor plate has been modeled according to an AR mechanism to provide different bubble patterns as reported by Whitehead.[29]

Bubble generation

Bubble formation phenomena will influence the distributor performance as well as the final bubble pattern developed within the bed; however, whereas bubble generation at a single orifice has been widely studied, and some models have been proposed for computing the bubble volume at the detachment,[26,30,31] to the authors' best knowledge, the information reported in literature regarding the multiorifice bubbling formation in gas–solid FBs is rather scarce.[32–34] In principle, the natural approach for multiorifice bubbling generation would be to address the case of multiple orifices as an extension of single-orifice bubble formation. However, several factors, such as gas leakage and the rapid formation of doublets and triplets by coalescence of the emerging bubbles, make the previous discrete bubble models appearing in the literature use instead empirical correlation to estimate the initial bubble size. Besides, other critical aspects of bubble formation, such as the bubble injection frequency and the subsequent injection pattern, have been often left out of the discussion. It is therefore clear that the bubble generation mechanism will play a major role, which must be addressed with caution to satisfactorily explain the observed performance of distributors in FBs.

In contrast to previous works, in this article, an extension of the single-orifice model proposed by Davidson and Harrison[26] will be used as a single-orifice departure model to further extend the bubble generation to a multiorifice distributor plate. According to that, at a superficial velocity greater than U_{mf}, the bubble volume formed at the orifice is given by:

$$V_0 = \frac{1.138 G^{1.2}}{g^{0.6}}, \tag{1}$$

where G accounts for the bubble flow per hole that within the proposed model reads as:

$$G = \frac{V_b}{N_{or}} = \frac{\psi U_e A_{bed}}{N_{or}}, \tag{2}$$

Next, the bubble frequency above the orifice can be estimated according to:

$$f_{b,or} = \frac{G}{V_0}, \tag{3}$$

Once both the bubble detachment volume and the bubble orifice frequency are estimated, the extension of the bubble generation to the multiorifice system is not trivial. As stated above, little is known about multiorifice bubbling, and previous reported works skip out of the discussion regarding the bubble injection patterns and the bubble generation frequency. Traditionally, due to the existing analogies between gas–liquid and gas–solid systems, the research carried on for gas–liquid mixtures is currently used to get knowledge on gas–solid FBs and vice versa. Accordingly, it can be argued that the few examples found in literature on multiorifice bubble generation dealing with uniform gas–liquid mixtures might be used to devise a multiorifice mechanism for FBs.[35] Thus, those studies explore how design and operation conditions such as pressure and plenum volume, orifice spacing, and liquid depth affect bubble size as well as bubbling synchronicity.[36] However, they are based on single-orifice models,[37] therefore, the gas flow through each orifice is determined from orifice equations, the estimated bubble volume is larger as pressure drop across the orifice increases. As a consequence, the higher the pressure drop, the larger the bubble will be. Moreover, the average gas flow thorough each orifice is obtained by dividing the gas flow rate by the total number of orifices, which leads to a decrease of the initial bubble size as increasing the orifice number. Apparently that approach holds for submerged single orifices in FBs,[31] however, when extrapolating to multiorifice generation, the direct implementation of that approach would conclude that the initial bubble size increases as the open area ratio

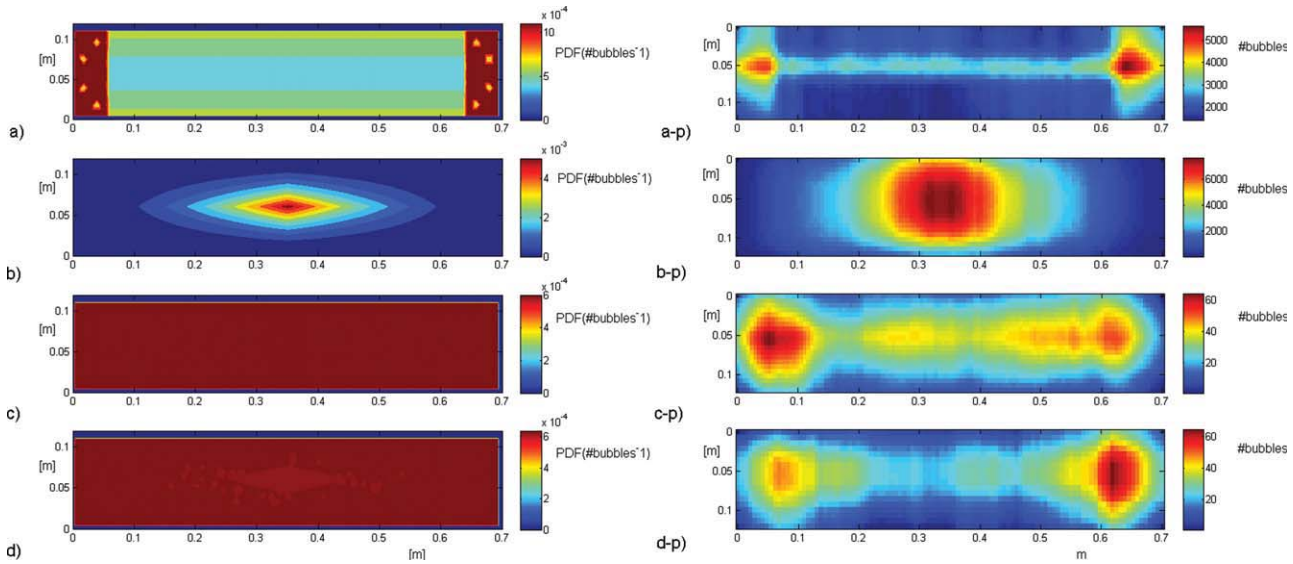

Figure 1. Bubble injection pattern, a, b, c, and d, and corresponding bubble dynamical structures developed within the bed, -p, used during the simulations.

The simulation corresponds to SBR conditions having $N_{or} = 1660$: (a, b) injection patterns with inactive bubble generation regions; (c) uniform gas distribution; and (d) modified uniform gas distribution to match Type 1 systems. [Color figure can be viewed in the online issue, which is available at wileyonlinelibrary.com.]

decreases, which is contrary to the experimental evidence on distributor performance that shows how bubble size increases when the open area is increased. In fact, it is well known that pressure drop across distributors indeed influences the bubble regime at low fluidization velocities.[38] Thus, for instance, it has been reported that a large pressure drop should lead to multiple bubble regime (MBR), which is characterized by many relatively small bubbles that are well distributed over the cross section of the bed, whereas for small pressure drops, single bubble regime (SBR) might appear. In that regime, the bubbles are larger in size and unevenly distributed over the cross section. Then, how to reconcile both the bubble generation mechanism and the distributor performance?

The activation region mechanism

The results reported on uniform gas–liquid systems[35,36] reveal that bubbling synchronicity is strongly influenced by the spacing and arrangement of the orifices, liquid depth, and gas flow rate; however, no explicit model is provided to account for that influence, which makes it very difficult to devise how the bubble synchronization can take place and consequently, nothing can be concluded about what to model; i.e., doublets, triplets, etc. However, those studies also report the fact that the orifices active in one part of the distributor enhanced the bubble generation within their nearest distributor region, making the orifices that belong to other distributor regions passive for bubble formation. Moreover, recently it has been reported that in the case of multiorifice distributors, for $U_0 > U_{mf}$ conditions, the region near the distributor plate exhibits permanent jets[34] and the bubble detachment occurs above that region. That information serves here to propose the AR mechanism, where the multiorifice plate is seen as a discrete source of information where the bubbles are the dynamical "message" to be transmitted, that sequence of bubbles follows a certain generation rate and injection pattern (Figures 1a–d). The injection pattern establishes the probability of bubble formation of the different distributor regions, consequently, the bubbles will be produced preferably on those orifices or tuyeres located within high-probability regions (red zones in Figures 1a–d) whereas low-probability regions (blue zones in Figures 1a–d) will produce less number of bubbles. According to that, Figures 1a–d show several injection patterns corresponding to different distributor conditions. Thus, Figures 1a, b present some injection patterns with inactive bubble generation regions, Figure 1c depicts a uniform gas distribution injection pattern, and finally, Figure 1d represents a modified version of the uniform gas distribution shown in Figure 1c. Complementarily to the injection patterns, Figure 1-p shows the resulting dynamical pattern developed within the bed depending of the injection pattern used during the simulation. Through this article, the injection pattern shown in Figure 1d has been used to match the behavior of distributor systems Type 1, as described by Whitehead[29] (Appendix). With regard to the generation rate it is assumed that in the same way in which the single orifice is characterized by a bubble injection frequency, $f_{b,or}$, the overall bubble generation frequency, f_b, characterizes the bubble generation rate at multiorifice distributors. According to that, the bubbles of size, v_b (i.e., active regions), will be generated at different locations on the distributor plate at a rate defined by f_b, where the initial bubble size is given by:

$$v_b = \frac{V_b}{f_b} \tag{4}$$

The AR approach assumes that the resulting initial bubble size, v_b (i.e., active region), is the consequence of the visible

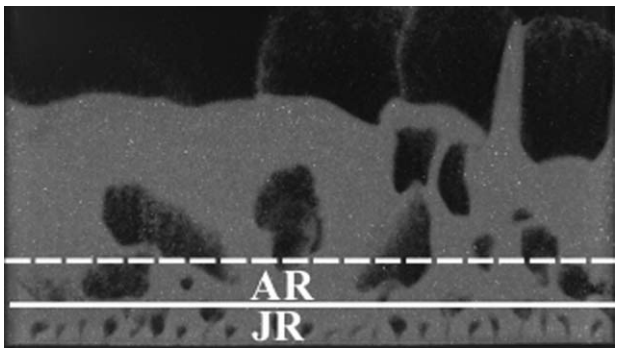

Figure 2. Two-dimensional fluidized bed operating at bubbling regime.

The solid line accounts for the limit of the orifice interaction region, JR; the active regions, i.e., bubbles, AR, will appear above the JR area.

bubble flow interaction of neighbor orifices, which means that during the bubble generation, it is assumed that all the visible bubble flow available for bubble formation at every time step is concentrated on a certain active region for bubble formation, the location of the generation point depends on the injection pattern (Figure 1d). Moreover, it is assumed that the active region (i.e., bubble) appears above the jet permanent area. Figure 2 shows a picture of an experimental 2D FB system operating at bubbling conditions with a multiorifice distributor, which serves to illustrate the idea behind the AR mechanism. Thus within the proposed model, the generated bubbles are the result of the interaction of neighbor orifices and will detach within the AR (Figure 2). The use of that approach makes the computational cost decrease significantly, which is an enormous advantage of the proposed methodology, and brings the opportunity to model large-scale beds in a common desktop computer in a timely manner. Moreover, to allow for this region activation mechanism to occur, the orifice frequency is assumed to be nonuniformly distributed over time. Finally, to estimate f_b, two different approaches are presented below, the synchronous and the asynchronous models.

The synchronous model

This generation approach does not include the distributor performance. Instead, the hypothesis underlying the synch approach assumes an ideal situation where every orifice of the multiorifice distributor produce bubbles simultaneously (synchronous generation) at $f_{b,or}$. Moreover, it is assumed that the orifice bubble generation frequency is uniformly distributed over time, and consequently, f_b equals $f_{b,or}$. However, due to the fact that the bubble generation frequency is directly derived from the orifice theory, when the design of the virtual distributor used in the model matches the real distributor, the model predicts erroneously the expected dynamical behavior of the bed unit.

Nevertheless, a generation approach where the effect of the distributor performance is not included can still be useful for dynamic diagnosis and dynamical matching. Thus, just by ignoring the distributor, the overall generation frequencies can be arbitrarily varied until matching the dynamical features experimentally observed in the FB under diagnosis, i.e., through pressure fluctuation measurement.

According to that, it is clear that to avoid the limitation of the synch model for designing purposes, the distributor performance needs to be taken into account.

The asynchronous model

To facilitate the use of the AR mechanism for designing purposes, the asynch approach assumes that the distributor performance will produce a deviation on the predicted $f_{b,or}$ by the previous synch model. Consequently, the overall bubble generation frequency will be given as:

$$f_b = \phi \cdot f_{b,or} \tag{5}$$

The challenge now is to estimate the deviation coefficient, ϕ, which should account for the distributor performance. It is clear that the operation of a distributor is closely related to its design, which will influence both the mixing of solids and the fluidization quality. A measure of the stirring effect of a distributor is the factor α_j.[27]

$$\alpha_j = \frac{\rho_g u_{or}^2/2}{\Delta P_b} \tag{6}$$

The factor α_j gives the relation between the kinetic energy of the orifice jets and the resistance of the bed, measured by the bed pressure drop, ΔP_b; u_{or} is the gas velocity through the orifice that, as it is well known, is closely related to the pressure drop across the distributor, ΔP_d. Thus, as ΔP_d increases, u_{or} increases and consequently, the stirring effect of the distributor, α_j, increases. It has been reported that when $\alpha_j > 1$, the stirring capacity of the distributor is mostly due to the jets formed at the orifices, whereas for $0.09 < \alpha_j < 1$, the stirring capacity is due to both jets and bubbles formed at the distributor, and finally, for $\alpha_j \ll 1$, the jets do not contribute much to the bed stirring and bubbles should do the job.

According to that, the stirring capacity of the distributor, α_D, should have at least two contributions: the contribution due to jet stirring, α_j, and the mixing promoted by the bubbles formed at the distributor, α_b. Thus, the methodology followed to estimate the deviation coefficient consists on computing the stirring capacity of the active area appearing at the distributor, α_{Da}, and later to extend that capacity to the rest of the distributor.

Once α_j have been calculated according to Eq. 6, by analogy to the jet stirring, the factor α_b accounts for the relation between the kinetic energy due to bubbles formed at the distributor plate and the resistance of the bed.

$$\alpha_b = \frac{\rho_e u_{b,or}^2/2}{\Delta P_b}, \tag{7}$$

where $u_{b,or}$ is the initial bubble velocity and it is estimated from the results of the synch model as:

$$u_{b,or} = \frac{d_{b0}}{2t_d}, \tag{8}$$

where d_{b0} includes the wake fraction, f_w, as:

$$d_{b0} = \left((1 + f_w) \cdot v_b \frac{6}{\pi} \right)^{1/3}, \quad (9)$$

where f_w is estimated according to Hoffmann et al.,[39] and t_d is the detachment time given by:

$$t_d = \frac{1}{g^{3/5}} \left(\frac{6V_b}{\pi} \right)^{1/5}, \quad (10)$$

Finally, the stirring capacity of the active area region of the distributor, α_{Da}, is given as the weighted mean of the two components:

$$\alpha_{Da} = w_j \alpha_j + w_b \alpha_b, \quad (11)$$

where the weights w_j and w_b are estimated as a first approximation as:

$$w_i = \frac{\alpha_i}{\alpha_j + \alpha_b}, \quad i = j, b, \quad (12)$$

The use of the weighted mean allows the jet component to dominate at high ΔP_d, whereas the bubble component dominates at low ΔP_d, being consistent with the observed experimental behavior. Finally, the deviation coefficient is computed by scaling the stirring capacity obtained from Eq. 11 to the overall distributor section.

$$\phi = \frac{\alpha_{Da}}{f_a}, \quad (13)$$

where f_a is the fraction of active area relative to the total distributor area that is estimated as:

$$f_a = \frac{\text{area of the active region}}{\text{bed area}} = \frac{\left(\frac{\pi}{4}\right) d_{b0}^2}{A_{bed}}, \quad (14)$$

Bubble rise

Following the results reported by Briongos et al.,[40] the proposed bubble model assumes that the bubbles are the driver of bubbling FBs dynamics, which is in agreement with previous approaches reported in literature.[23,24] In contrast to those previous models where the bubbles are considered as spherical elements, in the present approach, the bubbles are considered as spherical caps, which rise according to their size and local condition. Moreover, instead of computing the bubble trajectory by integrating the bubble velocity in time from empirical correlations, the bubbles are tracked individually according to Bokkers et al.,[25] where the virtual mass force has been modified to account for the spherical cap.[41]

$$\frac{d}{dt}[(m_b + m_v)U_b] = \left(\rho_g + C_v \rho_e\right) v_b \frac{d}{dt} U_b = F_B + F_D, \quad (15)$$

where F_B is the effective buoyancy force and F_D is the drag force acting on the bubble, which are given by:

$$F_g = -\frac{\pi d_b^3}{6} \rho_g g, \quad (16)$$

$$F_b = \frac{\pi d_b^3}{6} \left(\varepsilon \rho_g + (1 - \varepsilon)\rho_p\right) g, \quad (17)$$

$$F_B = F_b + F_g = \left(\frac{\pi d_b^3}{6}\right) \left(\rho_p - \rho_g\right) g (1 - \varepsilon), \quad (18)$$

$$F_D = -\frac{1}{2} C_D \rho_e \frac{\pi}{4} d_b^2 U_b^2, \quad (19)$$

According to Bokkers et al.,[25] the drag coefficient for single bubble rising is computed from the steady state force balance giving:

$$C_D = \frac{4}{3} \frac{\left(\rho_e - \rho_g\right)}{\rho_e} \frac{d_b g}{U_b}, \quad (20)$$

Thus, each bubble trajectory along the Z-axis is estimated by integrating Eq. 15, whereas the dynamical coupling between rising bubbles that lead to the XY displacement is driven by the wake acceleration force that results from the trailing bubble effect (Figure 3a).

Trailing bubble effect

The behavior of bubbles in FBs has received considerable attention, and expressions for estimating the rising velocities of bubbles have been previously reported.[42] Moreover, it is well known that bubbles rise more rapidly when rising in a bubble stream than in isolation due to the process of bubble coalescence.[43] Thus, the wake of the leading bubble accelerates the trailing bubble before the coalescence process takes place. Accordingly, it is clear that to simulate the observed bed behavior, the trailing effect should be taken into account to model the behavior of an interacting stream of bubbles. In previous works, the dynamical coupling between neighbors bubbles was either neglected[25] or described through empirical relationships.[23,24] In contrast, in this article, an interacting bubble model is proposed to describe the trailing bubble effect of the leading bubbles. The model is based on the pressure recovery in the wake below a spherical cap reported by Davidson and Harrison[26] and on the idea suggested by Clift and Grace[44] of adding to the isolated bubble velocity a component related to the particulate phase. The hypothesis is that the pressure drop originated by the wake of the leading bubble will cause acceleration of the corresponding trailing bubbles by means of a void propagation mechanism, thus the increase of velocity due to the wake acceleration force equals the velocity that the dense phase would have at the position of the trailing bubble.

According to that, the pressure recovery is obtained by applying Bernoulli's theorem to the system shown in Figure 3b.[26]

$$p_R = \rho_g g h - \frac{1}{2} \rho_g U_b^2, \quad (21)$$

Later Bernoulli's theorem is applied again to estimate the void propagation velocity that corresponds to the increase of bubble velocity due to the wake acceleration force (Figure 3c):

$$U_{void} = \sqrt{\frac{2p_R}{\rho_e}} \quad (22)$$

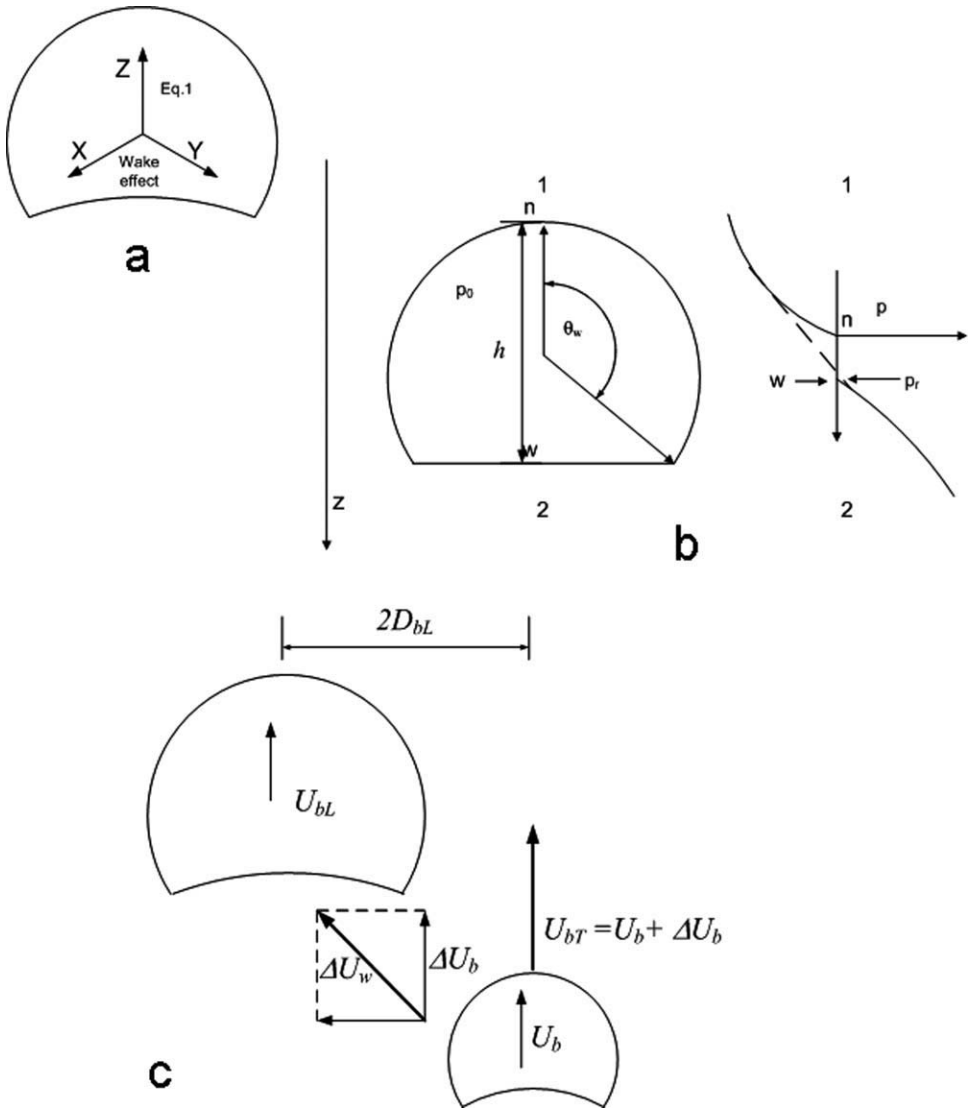

Figure 3. Spherical-cap discrete bubble model: (a) spherical cap, *X–Y* displacement is due to bubble interaction; (b) Pressure recovery phenomena; and (c) Trailing effect.

The bubble velocity of the trailing bubble is finally given as the sum of its isolation velocity plus the void propagation velocity:

$$U_{\mathrm{Tb}} = U_{\mathrm{ib}} + U_{\mathrm{void}} \tag{23}$$

Bubble coalescence

The coalescence of bubbles is modeled following the approach reported by Daw and Halow.[23] Consequently, during the coalescence, there is a net gas exchange between the lower and upper bubbles that governs the process. However, instead of defining the gas exchange rate, Q_c, as a function of bubble rise velocities, the through flow velocity across any plane through the bubble derived from the alternative analysis presented by Lockett et al.[45] is used as constant gas transfer rate during the coalescence, being therefore as:

$$Q_{\mathrm{c}} = 3U_{\mathrm{mf}}\frac{\pi}{4}d_{\mathrm{Lb}}^2, \tag{24}$$

Moreover, it is worth mentioning that neither the upper bubble nor the lower bubble are bound to the coalescence process; they are still free to interact with any neighbor bubble according to the phenomenological assumption presented below that ruled the interactions. That fact makes possible the splitting of the coalescing bubble pair to appear, giving rise to a final bubble size distribution resulting from coalescing, and splitting processes.

Other phenomenological key assumptions

(i) Bubbles grow only by coalescence.

(ii) Wall effects are not taken into account.

(iii) A bubble is a trailing bubble if it lies within the projected horizontal area defined by twice the diameter of its

Table 1. Experimental Condition Used Through the Simulations

Unit	Type of Distributor	N_{or}	d_{or} (m)	Size (m)	U_{mf} (m/s)	U_0 (m/s)	Bubble Regime	H_{bed} (m)	d_p (μm)	ρ_p (kg/m^3)	T (°C)
Cold Rig (Svensson et al. 1996a)	Perforate plate with triangular pitch	117	$2{\cdot}10^{-3}$	0.12 × 0.7	0.07	0.4	Multiple bubble Regime/single bubble regime/ exploding bubble regime	0.4/0.37	320	2600	20
		198							310		
		414				1.8		0.43			
		792				2.7					
		1660									
Bench Scale combustor	Nozzle with triangle pitch	28	$0.5{\cdot}10^{-3}$ (×20)	0.1 (ID)		0.14	Multiple bubble regime	0.28	346	2600	20
			0.28								

closest leading bubble, and if their center-to-center distance is less or equal than that of four times the leading bubble radii.[44]

(iv) For the coalescence processes to take place, the trajectory followed by the nose of the lower bubble should fall within the overlap region defined by one time the diameter of the upper bubble.

(v) Bubbles that are neighboring at horizontal level and do not fulfill the requirements for bubble coalescence are considered having its nose outside the coalescence region and therefore they rise without coalescence while moving side by side.[43–44]

(vi) When the nose of the lower bubble enters the wake of the leading bubble,[39] the coalescence process begins by shrinkage of the lower bubble and subsequent increase of the upper bubble. Coalescence will continue until the complete depletion of the lower bubble or until the splitting of the coalescing pair as a result of the interaction with neighbor rising bubbles.

(vii) Bubbles will exit the bed when their centers reach the bed surface.

(viii) Either when a bubble leaves the bed or when a bubble disappears as a result of the coalescence process, the total number of bubbles in the bed is reduced by 1.

Experimental Design

This article addresses the reliability of the proposed region activation model to simulate the dynamics of bubbling FB having either perforated plate or tuyere-type distributors (Table 1) and operating with B-Geldart particles. Accordingly, to validate the proposed approach, the dynamic characteristics of the simulated system are compared with both experimental and literature pressure fluctuation data. Thus, the cold rig used by both Johnsson et al.[8] and by Svensson et al.[38,46] to study the influence of pressure drop across the distributor on bottom bed regimes in CFBs, serves here for testing the reliability of the region activation model for designing purposes, and dynamic diagnosis matching of FBs having multiorifice distributors. Moreover, as an example of the use of the proposed model for tuyere-type systems, experimental data collected from a bench-scale combustor operating at ambient temperature are presented for model validation under current bubbling operating conditions. Most of the model settings used through the simulation and the fluidization unit characteristics are shown in Table 1.

Pressure fluctuation measurement

Multiorifice Distributor System. The experimental time series used during the validation of the multiorifice distributor model have been taken from Ref. 8; accordingly, the pressure time series were collected by means of a transducer Kistler Type 7261 placed at 0.2-m height connected to an adjustable range charge amplifier Type 5011A10, and the charge amplifier acts as a high-pass filter with a filter frequency of 0.1 Hz and only the fluctuating part of the signal was recorded. The sampling frequency used was 400 Hz for all fluctuating signals and 786,432 samples were taken corresponding to 33 min of total sampling time.

Tuyere Type System. The pressure fluctuations were measured by means of two pressure gauges PR3110 (Ellison Sensors) placed at two different positions: position 1 (0.1 m over the distributor) and position 2 (0.2 m near the bed surface), and connected to a PCI 6023E I/O board (National Instruments). The sampling frequency used was 200 Hz.

Simulated Time Series. The Davidson and Harrison model[26] is used to estimate the pressure time series. Thus, the pressure due to a single bubble passing a probe is estimated as:

$$P_b = \rho_s g(1-\varepsilon_{mf})\left(r - \frac{R_b^3}{r^2}\right)\cos\theta, \quad r \geq R_b \tag{25}$$

$$P_b = \rho_s g(1-\varepsilon_{mf}) r\cos\theta, \quad r < R_b \tag{26}$$

where R_b is the bubble radius and r is the distance from the bubble center to the pressure probe. Later, the simulated pressure time series caused by all the bubbles rising through the bed is estimated as the sum total of P_b:

$$P_m = \sum P_b \tag{27}$$

Besides the simulated time series, other relevant information such as the bed height fluctuation, void fraction, bubble size, and angle of gyration[24] are collected to help the dynamic diagnosis.

Results

Perforated plate distributor

The validation of the proposed approach for designing and dynamic diagnosis of gas–solid FBs having a multiorifice distributor undergoes two steps. First, the influence of the pressure drop across the air distributor is studied by comparison of the simulated data with the results reported by Svensson et al.,[38] for bottom bed regimes appearing in circulating FBs, CFBs. Later, a detailed dynamical comparison between the dynamics characterizing the simulated time series and the Kistler pressure fluctuation data reported by Johnsson et al.[8] is performed to study the different

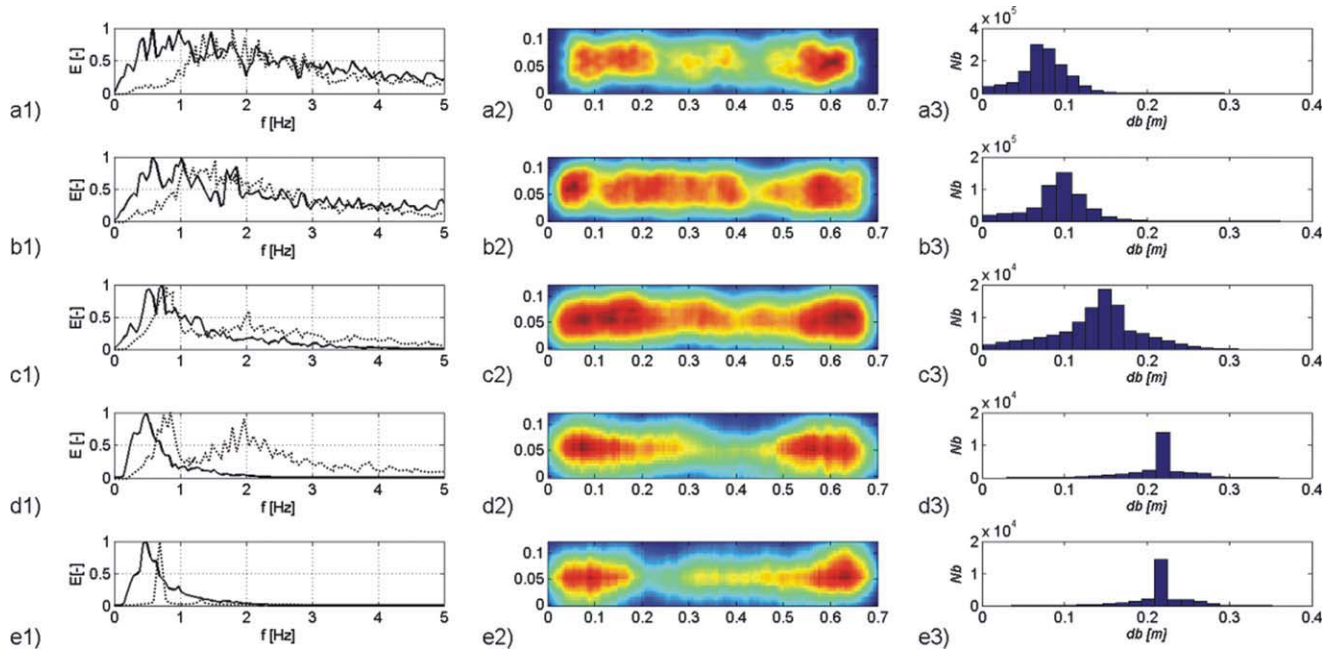

Figure 4. Influence of pressure drop across the air distributor: (a1, b1, c1, d1, and e1) power spectra (model: solid line; experimental: dot line) for distributor plates having, respectively, N_{or} = 117, 198, 414, 792, and 1660; (a2, b2, c2, e2, and d2) corresponding bubble patterns developed within the bed; (a3, b3, c3, d3, e3) bubble size histogram.

The fluidization velocity was 0.4 m/s, $h_f = 0.55$ m; $d_p = 320$ μm. [Color figure can be viewed in the online issue, which is available at wileyonlinelibrary.com.]

dynamical scales appearing in the model. Thus, frequency domain, stated space analysis, mutual information function (MIF), and multiresolution analysis by applying the empirical method of decomposition (EMD)[9] are complementarily used to perform the comparison between both the simulated and the measured pressure fluctuation data.

The simulated cold rig has a cross section of 0.12 × 0.70 m having five different perforated plates (Table 1), the bed material is silica sand particles of 320 and 300 μm in size, respectively, and the virtual pressure probes are located at 0.05 m, 0.15 (0.2) m. Moreover, other model outputs are the pressure drop fluctuation which is estimated as: $\Delta P = \rho_p(1 - \varepsilon_f)gh_f$, the bed height, h_f, the void fraction, ε_f, and the nondimensional cross-sectional area of the bubble stream, A_r^*.[24]

The influence of pressure drop across the air distributor

Figures 4a1–e1 compare the power spectra estimated from the simulated pressure fluctuation time series (solid line) with the power spectra reported in Ref. 38 for similar operating conditions (dot line). It can be seen how the pressure drop of the air distributor, Δp_{dist}, influences the fluidization behavior of the bed at low fluidization velocities. Thus, as same as the results reported by Svensson et al.,[38] large Δp_{dist} (low number of orifices) lead to MBR (Figures 4a1–c1), which is characterized for a wide range of relatively high frequencies up to 3 Hz, whereas low Δp_{dist} lead to SBR (Figures 4d1–e1), which exhibits a sharp peak below 1 Hz. Moreover, Figures 4a2–e2 and 4a3–e3 show, respectively, how the pressure drop influences both the bubble pattern and the bubble size distribution promoted within the bed. It is worth to point out that despite the direct comparison of the simulated and measured signals in the frequency domain reflects a high degree of similarity for some bubbling conditions, as discussed below; a multiscale approach should be used instead for a detailed comparison between simulated and measured data. Nevertheless, from a visual comparison of the simulated data with the experimental data[38] shown in Figures 4a1–e1, it might be concluded that the proposed model apparently provides a reliable quantitative and qualitative description of the measured bubbling FB dynamics. Moreover, it is worth to point out that the sampling frequency used by Svensson et al.[38] was 20 Hz, which is enough to collect the low-frequency dynamical information below 2 Hz but insufficient to explore the high-frequency dynamical regions reported later for the same test rig by Johnsson et al.[8] According to that, from a detailed dynamical comparison of the simulated data, the results reported by Johnsson et al.[8] are more suitable as they were measured by using high-sensitive pressure transducer and a sampling frequency of 400 Hz. Moreover, Figure 4 serves to illustrate the potential use of the proposed model for scale-up or extrapolation. Thus, as the bubble dynamics is the driver of the bed dynamics, the resulting macroscale flow structures characterizing the corresponding bubble patterns shown in Figures 4a2–e2, which determine the large-scale mixing behavior of the FB, reveal if the gas phase is well distributed or if in contrast, there is a maldistribution of the gas phase and consequently, some action to manipulate the resulting macroscale flow structures should be taken.

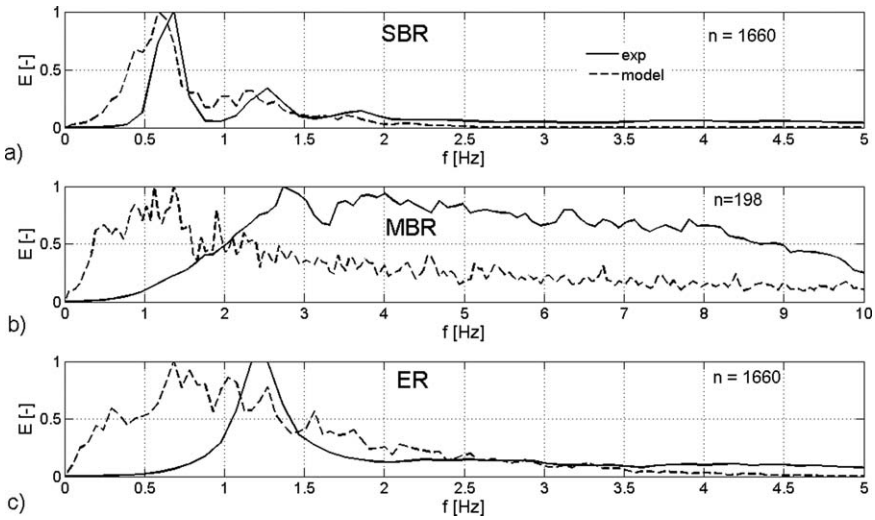

Figure 5. Comparison of the simulated signal with the measured Kistler pressure signal used in Ref. 8.

(a) Single bubble regime; (b) Multiple bubble regime; and (c) Exploding bubble regime.

Figure 5 shows the power spectrum for both the simulated data and the experimental time series used by Johnsson et al.[8] for either single, multiple or exploding bubble regimes (ERs). It can be observed how the model apparently matches the measured dynamics for SBR, whereas it exhibits clear differences for both the MBR and for the ER. In contrast to the previous results reported in literature, where the MBR was characterized by frequencies up to 3 Hz (Figure 4a1, dot line), the experimental MBR spectrum shown in Figure 5 exhibits frequencies ranging approximately up to 10 Hz. The high sensitivity of the pressure transducer and the larger sampling frequency used facilitate the collection of more dynamical information within the high-frequency region, which is attributed to dense-phase dynamical processes, which are mainly due to the dynamic interactions between the bubble and the dense phase. The fact that those interactions are not explicitly modeled, make the simulated pressure signals, which are derived from the bubbles existing within the bed, Eq. 27, carry information ruled by the bubble dynamics, and that they just contain little information about the global bed motion through the effect of bed height fluctuation on bubble rise dynamics (Eq. 18). Consequently, the simulated time series are mainly characterized by low-frequency components. Therefore, the direct comparison between the simulated data and the experimental pressure fluctuation time series for both the MBR and the ER, whose dynamics are strongly influenced by dense-phase processes, would be biased due to the strong influence which the high-frequency components have on the measured signals. Accordingly, instead of direct comparison, a multiscale analysis is proposed to use to compare the corresponding low-frequency dynamics of both simulated and experimental pressure time series collected at MBR and ER conditions.

The SBR has been identified when the FB operates with a low pressure drop of the air distributor. Moreover, it has been reported that the gas flow apparently exhibits a discontinuous behavior ruled by the bubble dynamics, being therefore, the formation and eruption of large bubbles of the dynamical feature which characterizes this regime.[46] According to that, as expected, Figure 5a shows a strong dynamic similarity between the simulated and the experimental pressure time series, as in essence the proposed model is based on formation, interaction, and eruption of bubbles. Consequently, there is no need to perform a multiscale approach to validate the model performance for SBR conditions, the direct comparison between the measured signal and the simulated time series suffices to point out the remarkable matching between the compared signals. Accordingly, the frequency domain analysis shown in Figure 5a reveals that both the exploding bubble frequency (low-frequency peak), due to bubble dynamics, and the single bubble frequency peak corresponding to the natural bed frequency matches. However, as the mutual information analysis shown in Figure 6,[47] both the simulated and the measured time series have differences within their short-term temporal structure. Thus, the MIF of the measured signal exhibits persistence corresponding to the high-frequency peak, observed during the frequency domain analysis, where as such persistence appears attenuated within the simulated data. As stated above, the simulated pressure time series lacks information concerning dense-phase phenomena, and only the bed height fluctuation slightly influences the simulated signal through the void fraction, ε, in Eq. 18. Consequently, the bulk dynamics[9] is responsible for the differences within the short-term temporal structure between both the measured and the simulated pressure time series observed in Figure 6.

Complementarily to the frequency domain and mutual information analyses, the state space analysis has been used to validate the model. Thus, Figure 7 shows the principal component analysis (PCA) and the eigenvalue spectra estimated according to the Broomhead and King method.[48] As expected from the previous analysis, the resulting attractor structure and eigenvalue spectra for both the simulated and the measured pressure time series are very similar. Moreover, other traditional nonlinear measures such as the correlation dimension, D_2,[49] and the Kolmogorov entropy per cycle, K_c,[50] shown in Figure 7, are consistent with the expected values. Consequently, the measured pressure time series are characterized by a Kolmogorov

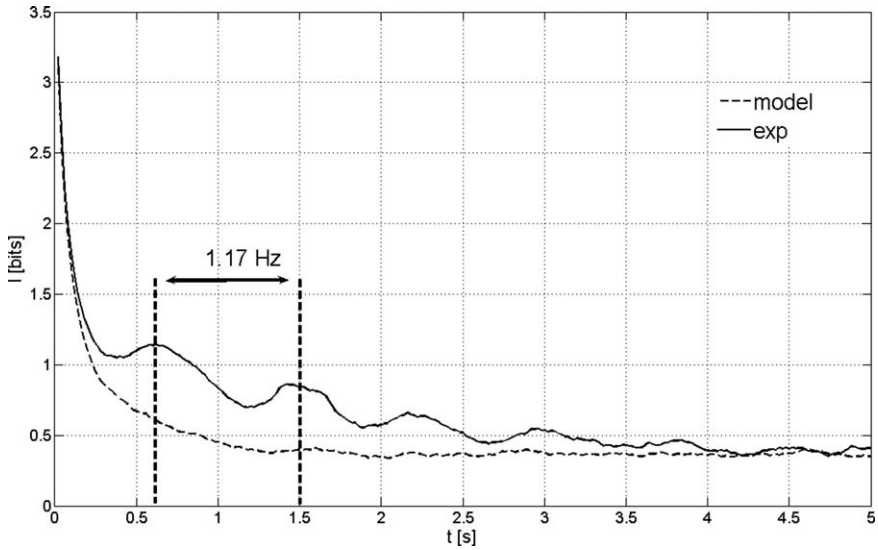

Figure 6. Mutual information function analysis for simulated and measured signal taken at SBR conditions.

Note the short-term difference between experimental and simulated data.

entropy lower than the value estimated from the simulated time series, as a consequence of the persistence occurring at short-term scale. Moreover, the high degree of similarity between the reconstructed attractors is confirmed by the same value of the correlation dimension, which, as it is well known, is a measure of spatial homogeneity.

As stated above, a multiscale approach is needed for comparison when operating at MBR. Consequently, to properly compare the low-frequency dynamics of the simulated and the measured pressure fluctuation signals, the Hilbert–Huang transform method (HHTM) is used to extract the information below the natural bed frequency. Thus, once the original time series have been decomposed into a finite number, n, of intrinsic mode functions (IMFs), associated with various time scales and the residual r_n, the time series of interest can be reconstructed as a surrogate of the original time series by superposition of the IMFs, $C_n(t)$, and the residual up to the bulk dynamic level as:

$$x(t) = \sum_{j=1}^{n=\text{bulk}} C_j(t) + r_n \tag{28}$$

where $C_{\text{bulk}}(t)$ corresponds to the global bed motion caused by the gravitational oscillations of the FB material, which is characterized by the natural bed frequency.

Table 2 shows the averaged instantaneous frequencies estimated according to Briongos et al.[9] for the five modes

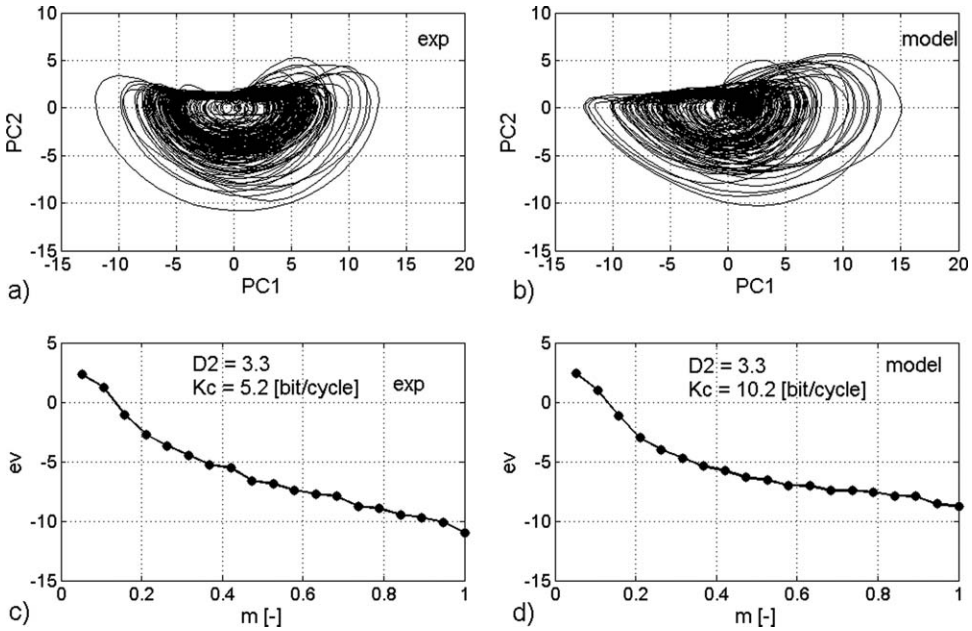

Figure 7. State space analysis of the experimental and the simulated pressure time series at SBR conditions: (a, b) reconstructed attractors; (c, d) eigenvalue spectra.

Table 2. Averaged Instantaneous Frequencies for Five Modes Corresponding to the Simulated and Measured Time Series Extracted, at Multiple Bubble Regime, Through the EMD Process

	$\langle w_1 \rangle$ (Hz)	$\langle w_2 \rangle$ (Hz)	$\langle w_3 \rangle$ (Hz)	$\langle w_4 \rangle$ (Hz)	$\langle w_5 \rangle$ (Hz)
Measured signal	5.94	2.81	**1.36**	0.54	0.20
Simulated signal	7.16	3.76	1.74	**0.76**	0.32

corresponding to the simulated and measured MBR extracted through the EMD process. The stopping criterion has been set by the way in which the sifting process is stopped when the averaged instantaneous frequency of the current mode is smaller than the characteristic bubble exploding frequency (0.5 Hz). According to that, the mode $<w_5>$ of Table 2 is the lower dynamical level drawn from the analysis.

As stated before, once the EMD process terminates, a "low-pass" filtered version, x_f, of both the simulated and the measured time series is reconstructed following Eq. 28 by superposition of the IMFs and the residual up to the bulk dynamic component. To estimate the natural bed frequency, f_{bulk}, a conventional expression previously reported in literature such as that of Baskakov et al.,[51] $f_{bulk} = 1.5$ Hz might be used; however, in this case, it is concluded from Figure 5 that the model proposed by Roy et al.[52] almost matches the natural bed frequency, $f_{bulk} = 1.1$ Hz. Consequently, the bulk dynamic component is the one which has the average instantaneous frequency closest to f_{bulk} (Table 2, bold frequencies).

Figure 8 compares the temporal structure of the measured and the simulated surrogate time series by means of the power spectra and the MIF. As for the case of SBR, the power spectra are very similar, being the model spectra slightly shifted toward lower frequencies (Figure 8a). Moreover, the mutual information analysis matches, pointing out a high degree of dynamical similarity between the measured and the simulated dynamics (Figure 8b). Concluding with the dynamical comparison, the results from the state space analysis confirm the high degree of similarity between the compared dynamics (Figure 9). Thus, the reconstructed attractor, eigenvalue spectra, and attractor properties such as the correlation dimension and Kolmogorov entropy almost match. Therefore, it is concluded that the simulated time series preserves both the linear and the nonlinear features of the measured dynamics.

In contrast to the SBR and MBR, the experimental evidence shows that ER occurs at gas velocities that are several times as high as the terminal velocity of the averaged bed particle size,[38,46] under such fluidization conditions, the bottom bed dynamics is characterized by large irregular voids that promote a vigorous interaction with the dense phase. Figure 10a shows the power spectra of the simulated pressure time series. It can be observed that it is not just a shifted delay version of the experimental run, as was observed in the case of the MBR, now the power spectra for both surrogates of the simulated and the measured pressure time series are different. Moreover, as for the SBR case, the MIF exhibits differences within the short-term temporal structure (Figure 10b). Thus at short-term scale, the MIF of the measured dynamics exhibits a minimum around 0.3 s whereas the simulated time series does not show any singular point and instead of that, its MIF smoothly decreases reaching its long-term memory value, which matches that of

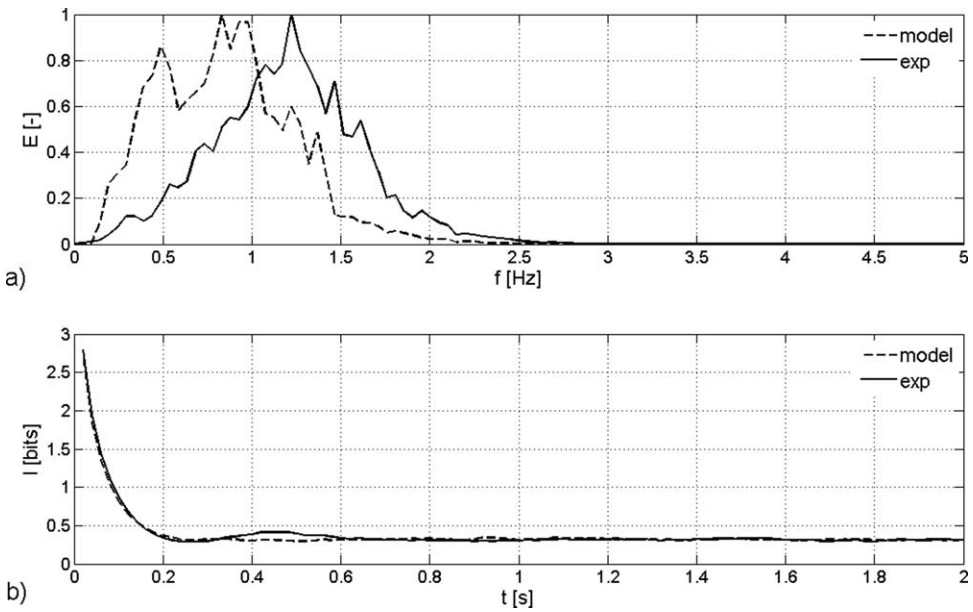

Figure 8. Time structure comparison for the surrogate signals obtained from the multiresolution analysis applied over the measured and the simulated pressure time series for multiple bubble regime: (a) frequency domain comparison; (b) mutual information function analysis.

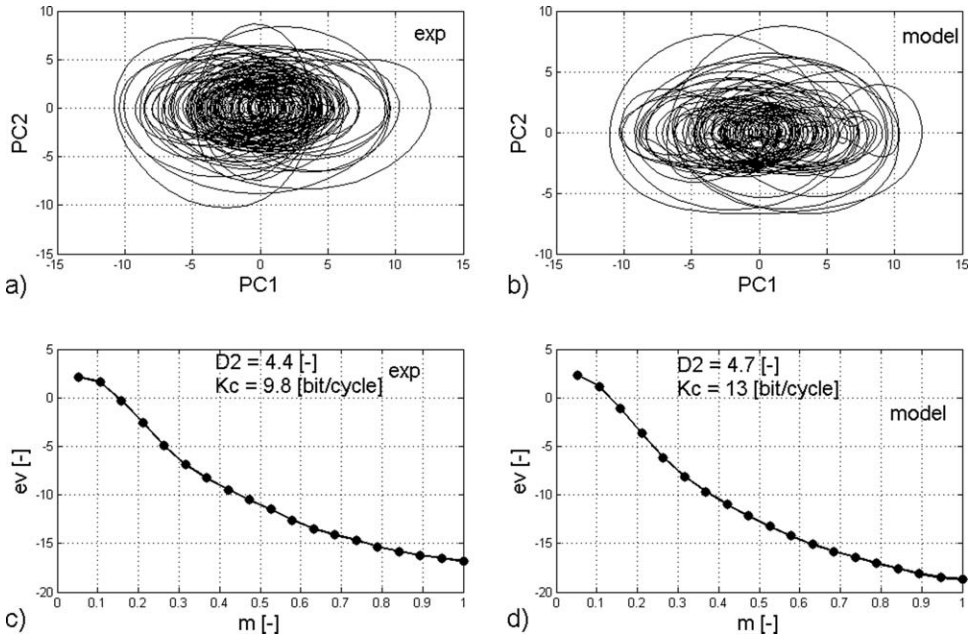

Figure 9. State space analysis for the surrogate signals for multiple bubble regime: (a, b) reconstructed attractors; (c, d) eigenvalue spectra.

the measured dynamics. According to that, as for the SBR, the similarities within the long-term temporal structure are confirmed through the state space analysis. Thus, when comparing the reconstructed attractors for both surrogates, it can be observed how the simulated PCA projection mimics both the shape and size of the core of the experimental reconstructed attractor (Figure 11). The slight differences between both projections, which are mainly due to the absence of outer orbits around the core of the reconstructed attractors from simulated signal, is explained by differences exhibited within the short-term temporal structure (Figure 10b), which comes from high-frequency dense-phase phenomena that are not taken into account by the model (Figure 10a). Moreover, the values of the Kolmogorov entropy and correlation dimension of the simulated pressure time series are very close to those of the measured signal.

Finally, in agreement with the results reported in literature,[38,46] the simulated exploding bubble dynamics is independent of the distributor pressure drop, consequently, similar results are obtained when comparing simulated time series obtained for ER conditions by using different distributor pressure drops (Figure 12).

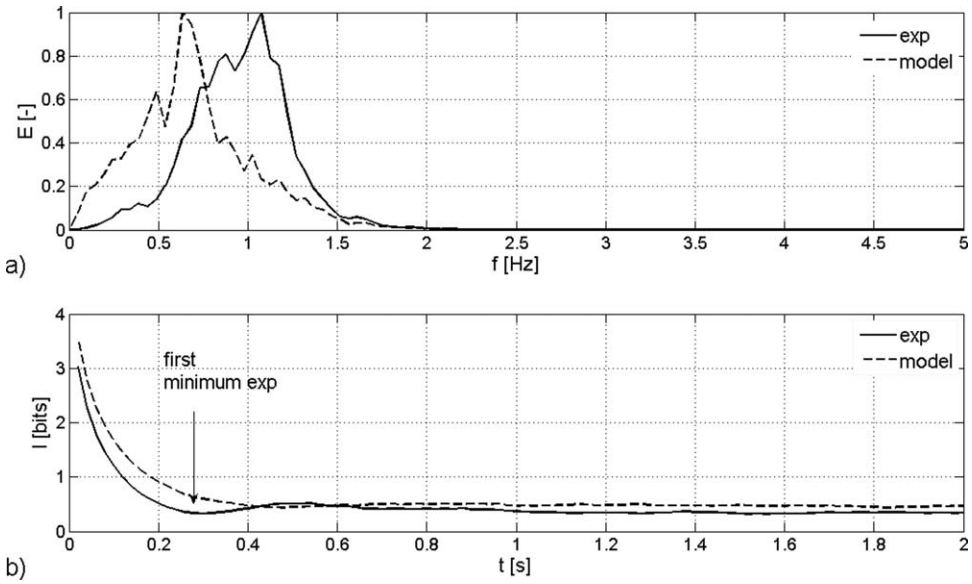

Figure 10. Time structure comparison for the surrogate signals for exploding bubble regime: (a) frequency domain comparison; (b) mutual information function analysis.

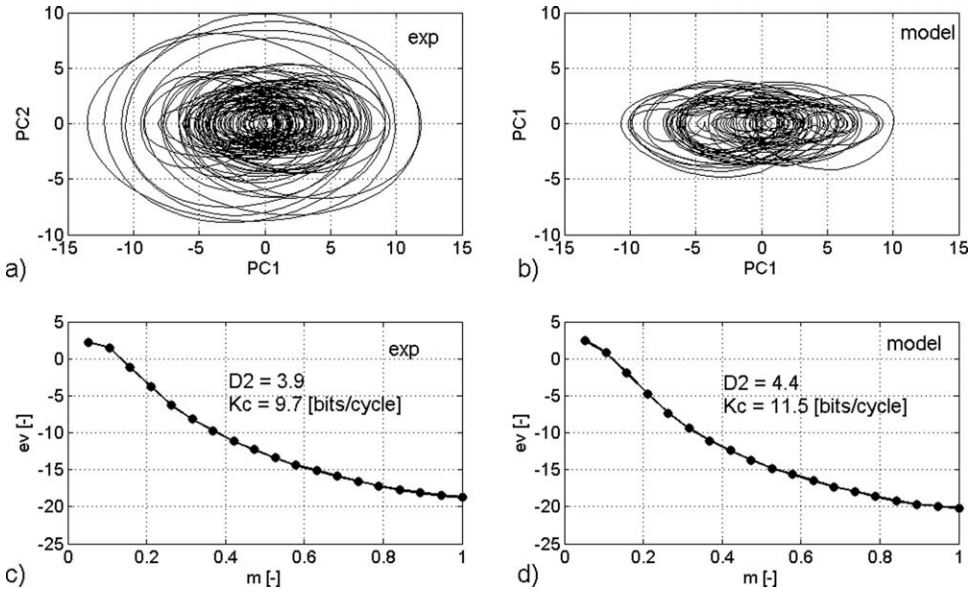

Figure 11. State space analysis for the surrogate signals for exploding bubble regime: (a, b) reconstructed attractors; (c, d) eigenvalue spectra.

Tuyere plate distributor

Since perforated plate distributors cannot be used under severe operating conditions, other designs such as tuyere plate distributors are used in those situations; therefore, due to the fact that many industrial processes use those distributor types, it is worth testing the reliability of the proposed approach to deal with the modeling of bubbling FBs operating with tuyere plate distributors. Accordingly, as an example of the use of the proposed model for tuyere-type systems, the performance of a bench-scale combustor operating at ambient temperature is presented for model validation under current bubbling operating conditions (Table 1).

The validation of the proposed model for dynamic diagnosis and design of gas–solid FBs having a tuyere plate distributor follows the same methodology previously used for MBR and ER analysis. Thus, the power spectra of both the measured and the simulated time series are shown in Figure 13a. Let us note that due to the fact that the pressure sensor used to monitor the bench-scale combustor is less sensitive than the Kistler pressure transducer, the direct comparison of the signals in the frequency domain reflects a high degree of similarity in MBR. However, as the MBR is characterized by an intense dynamical interaction between the bubble and the dense phase, which is not taken into account by the model, the same multiscale approach as in the case of multiorifice distributor is used here for a detailed comparison when operating at MBR. Consequently, the HHTM is used to extract the information below the natural bed frequency. Subsequently, surrogates of the original time series are reconstructed by superposition of the IMFs and the residual up to the bulk dynamic level. It is clear from Figure 13b that as same as in the multiorifice distributor case, the power spectra of the compared surrogates almost match, moreover, the results from the MIF analysis confirm that both time series have a similar temporal structure; therefore, as expected, the subsequent state space analysis match, indeed it can be seen in Figure 14 how the attractor structure as well as its invariants remain the same for both the simulated and experimental data, which confirms the reliability of the model also for tuyere-type systems.

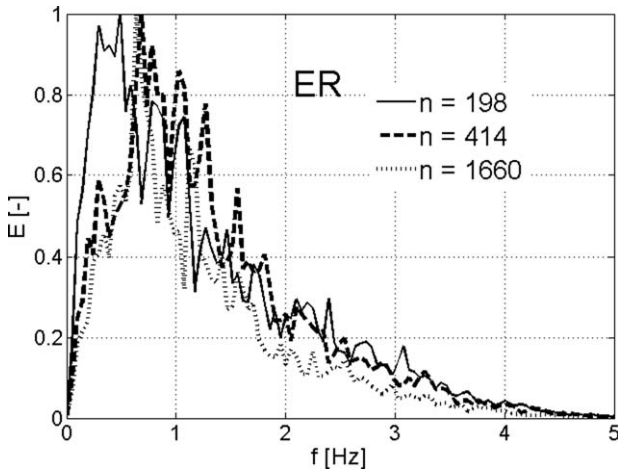

Figure 12. Power spectra of simulated time series obtained for exploding regime operating conditions having distributor plate with N_{or} = 198, 414, and 1660, respectively.

Conclusions

The proposed bubble-cap model operated either with the synchronous bubble generation mechanism (user defined overall bubble generation frequency) or with the asynchronous bubble generation model (distributor performance correction) matches the dynamic characteristics of bubble dynamics found on gas–solid FBs operating either at multiple or at SBRs, with gas velocities ranging between $2 < U_r < 6$, or at large fluidization velocities when the bed operates at exploding regime.

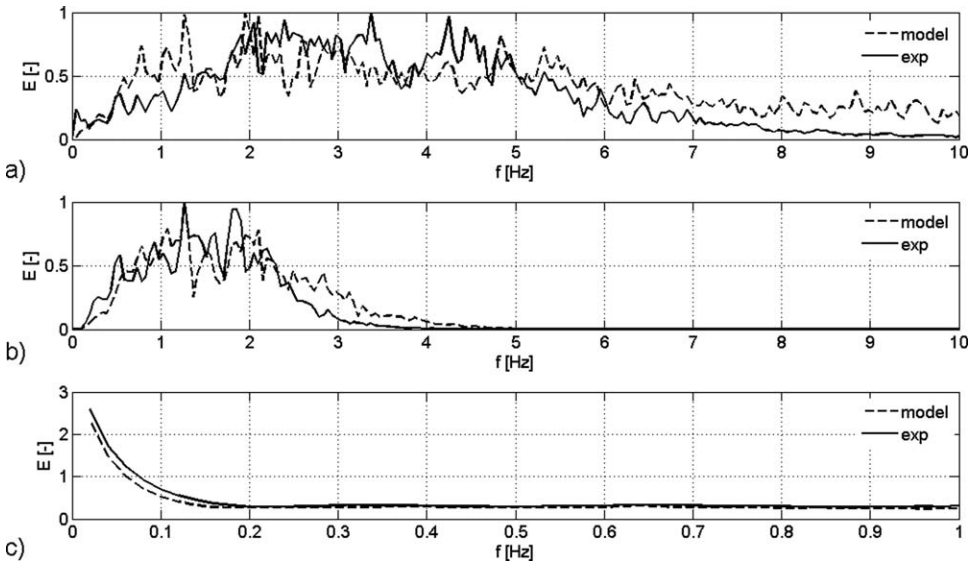

Figure 13. Time structure comparison for the tuyere-type system operating at multiple bubble regime: (a) frequency domain comparison of the measured and simulated pressure signals; (b) power spectra of surrogate signals; and (c) mutual information function analysis over the surrogates.

The AR mechanism, resulting from the asynchronous bubble generation, makes it possible that the model accounts for the effect of the distributor performance due to the influence of the pressure drop across the distributor plate on bed regimes. Moreover, the model serves to simulate gas–solid FBs having either multiorifice or tuyere-type distributors, being a useful tool to be applied to help in the design and operation of bubbling FBs.

Through the multiscale nonlinear approach used for model validation, some dynamical aspect characteristics of bubbling dynamics such as exploding bubble phenomena have been identified by establishing a direct relation between the physical phenomena driving the dynamics (bubble generation, interaction, and eruption) and the measured signals.

The asynchronous approach opens the possibility of using the proposed model for scale-up and design purposes. In one hand, design aspect such as distributor effect or fluidization conditions has been covered when comparing the dynamics predicted by the proposed model with the dynamics measured from different facilities operating at different fluidization conditions. On the other hand, as the proposed approach lacks of computational size restrictions, the use of the proposed model for scale-up processes is straightforward, the only requisite is to have a full description of the distributor design and operating conditions.

Finally, although the results are very promising, the model has been tested only with cold bed installations and more research is needed to get an insight into multiorifice bubble distribution and hot bed facilities.

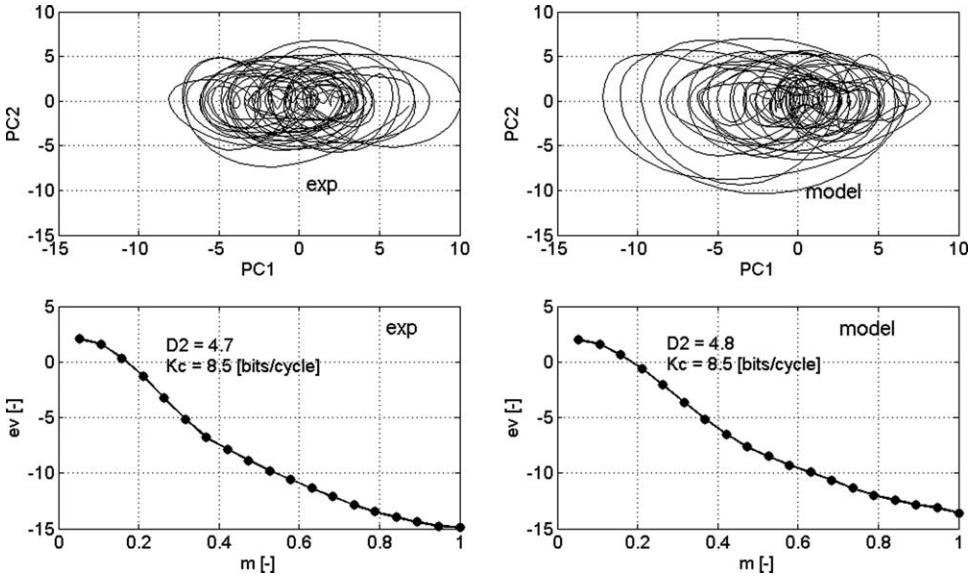

Figure 14. State space analysis for the surrogate signals of the tuyere-type system at multiple bubble regime: (a, b) reconstructed attractors; (c, d) eigenvalue spectra.

Acknowledgments

The author would like to specially thank Prof. Filip Johnsson (Chalmers University) who kindly provided the Kistler pressure time series for model validation. Besides the financial support from projects DPI2009-10518 (MICINN) and CARDENER-CM (S2009ENE-1660) is very much acknowledged.

Notation

A_{bed} = bed area, m^2
C_j = IMF component
C_v = virtual mass force coefficient
D_2 = correlation dimension
d_{b0} = initial bubble size from synch approach, m
d_b = bubble diameter, m
d_{Lb} = leading bubble diameter, m
E = power spectrum energy
ev = normalized eigenvalue[53]
f_a = fraction of active area
f_b = overall bubble generation frequency, Hz
$f_{b,or}$ = bubble orifice frequency, Hz
f_w = wake fraction
G = bubble flow per hole, m^3/s
h_f = bed height, m
I = mutual information function, bits
K_c = Kolmogorov entropy per cycle, bits per cycle
m = dimensionless embedding dimension
N_b = Number of bubbles in the histogram
N_{or} = Number of orifices
p_R = pressure recovery, Pa
Q_c = gas transfer rate during coalescence, m^3/s
R_b = bubble radius, m
r = bubble to pressure probe distance, m
r_n = decomposition residual
t_d = bubble detachment time, s
U_b = bubble velocity, m/s
U_{ib} = isolation bubble velocity, m/s
U_0 = superficial gas velocity, m/s
U_{mf} = minimum fluidization velocity, m/s
U_{tb} = trailing bubble velocity, m/s
U_{void} = void propagation velocity, m/s
$u_{b,or}$ = initial bubble velocity from synch approach, m/s
u_{or} = gas velocity through the orifice, m/s
V_b = visible bubble flow, m^3/s
v_b = bubble size of active region, m^3

Greek letters

α_b = stirring factor due to bubbles
$\alpha_{D,a}$ = stirring capacity of the active area region
α_j = stirring factor due to jets
ε_f = void fraction
ϕ = deviation coefficient from synch approach
θ = angle between vector from origin to pressure probe tip and the positive vertical axis
ρ_g = gas density, kg/m^3
ρ_e = emulsion density, kg/m^3
ρ_p = particle density, kg/m^3
ψ = dimensionless ratio between observed bubble flow and the excess flow

Abbreviations

CBF = circulating fluidized bed
EMD = empirical mode decomposition
ER = exploding bubble regime
HHTM = Hilbert–Huang transform method
IMF = intrinsic mode function
MBR = multiple bubble regime
MIF = mutual information function analysis
PCA = principal component analysis
SBR = single bubble regime

Literature Cited

1. Jonhsson F. Fluidized bed combustion for clean energy. In: Proceedings of the 12th International Conference on Fluidization, Vancouver, Candada, 2007:47–62.
2. Cui H, Grace JR. Fluidization of biomass particles: a review of experimental multiphase flow aspects. *Chem Eng Sci*. 2007;62:45–55.
3. Werther J. Measurement techniques in fluidized beds. *Powder Technol*. 1999;102:15–36.
4. Briongos JV, Guardiola J. Free top fluidized bed surface fluctuations as a source of hydrodynamic data. *Powder Technol*. 2003;134:133–144.
5. Dyakowski T, Jeanmeure LFC, Jaworski AJ. Applications of electrical tomography for gas-solids and liquid-solids flows—a review. *Powder Technol*. 2000;112:174–192.
6. Briongos JV, Aragón JM, Palancar MC. Fluidised bed dynamics diagnosis from measurements of low frequency out bed passive acoustic emissions. *Powder Technol*. 2006;162:145–156.
7. Van Ommen JR, Mudde RF. Measuring the gas-solids distribution in fluidized beds—a review. In: Proceedings of the 12th International Conference on Fluidization, Vancouver, Candada,2007:31–46.
8. Johnsson F, Zjierveld RC, Schouten JC, van den Bleek CM. Characterization of fluidization regimes by time-series analysis of pressure fluctuations. *Int J Multiphase Flow*. 2000;26:663–715.
9. Briongos JV, Aragón JM, Palancar MC. Phase space structure and multi-resolution analysis of gas solid fluidized beds hydrodynamics. Part I: the EMD approach. *Chem Eng Sci*. 2006;61:6963–6980.
10. Fiorentino F, Marzocchela A, Salatino P. Segregation of fuel particles and volatile matter during devolatilization in a fluidized bed reactor-I. Model development. *Chem Eng Sci*. 1997;52:1909–1922.
11. Gidaspow D. *Multiphase Flow and Fluidization*. San Diego: Academic Press, 1994.
12. Ding J, Gidaspow D. A bubbling fluidization model using kinetic theory of granular flow. *AIChE J*. 1991;36:523–538.
13. Van Wachem BGM, Schouten JC, van den Bleek CM, Krishna R, Sinclair JL. Comparative analysis of CFD models of dense gas-solid systems. *AIChE J*. 2001;47:1035–1051.
14. Lindborg H, Lysberg M, Jakobsen HA. Practical validation of the two-fluid model applied to dense gas-solid flows in fluidized beds. *Chem Eng Sci*. 2007;62:5854–5869.
15. Deen NG, van Sint Annaland M, van der Hoef MA, Kuipers JAM. Review of discrete particle modeling of fluidized beds. *Chem Eng Sci*. 2007;62:28–44.
16. Tsuji T, Yabumoto K, Tanaka T. Spontaneous structures in three-dimensional bubbling gas-fluidized bed by parallel DEM–CFD coupling simulation. *Powder Technol*. 2008;184:132–140.
17. Sundaresan S. Modeling the hydrodynamics of multiphase flow reactors: current status and challenges. *AIChE J*. 2000;46:1102–1105.
18. Wang J, Van der Hoef MA, Kuipers JAM. Coarse grid simulation of bed expansion characteristics of industrial-scale gas-solid fluidized beds. *Chem Eng Sci*. 2010;65:2125–2131.
19. Grace JR, Taghipour F. Verification and validation of CFD models and dynamic similarity for fluidized beds. *Powder Technol*. 2004; 139:99–110.
20. Sasic S, Leckner B, Johnsson F. Time–frequency investigation of different modes of bubble flow in a gas–solid fluidized bed. *Chem Eng J*. 2006;121:27–35.
21. Van Wachem BGM, Schouten JC, Krishna R, van den Bleeck CM. Validation of the Eulerian simulated dynamic behaviour of gas-solid fluidized beds. *Chem Eng Sci*. 1999;54:2141–2149.
22. Van den Bleek CM, Schouten JC. Can deterministic chaos create order in a fluidized-bed scale-up. *Chem Eng Sci*. 1993;48:2367–2373.
23. Daw CS, Halow JS. Modelling deterministic chaos in gas fluidized beds. *AIChE Symp Ser*. 1992;88:61–69.
24. Pannala S, Daw CS, Halow JS. Dynamic interacting bubble simulation (DIBS): an agent-based bubble model for reacting fluidized beds. *Chaos*. 2004;14:487–498.
25. Bokkers GA, Laverman JA, van Sint Annaland M, Kuipers JAM. Modelling of large-sclae dense gas-solid bubbling fluidised beds using a novel discrete bubble model. *Chem Eng Sci*. 2006;61:5590–5602.
26. Davidson JF, Harrison D. *Fluidised Particles*: Cambridge University Press, 1963.
27. Kunii D, Levenspiel O. *Fluidization Engineering*. MA: Butterworth-Heinemann, 1991.

28. Johnsson F, Andersson S, Leckner B. Expansion of a freely bubbling fluidized bed. *Powder Technol*. 1991;68:117–123.
29. Whitehead AB. *Distributor characteristics and bed properties*. In: *Fluidization*. Chapter 5, edited by Davidson JF, Clift R and Harrison D. Second edition, 1985, London, U.K.: Academic Press. pp. 173–198.
30. Caram HS, Hsu K-K. Bubble formation and gas leakage in fluidized beds. *Chem Eng Sci*. 1986;41:1445–1453.
31. Vakhshouri K, Grace JR. Modeling of bubble formation at a submerge orifice in gas-fluidized bed. *Chem Eng Res Des*. 2009;87: 843–851.
32. Leung LS. Design gas distributor and prediction of bubble size in large gas-solids fluidized beds. *Powder Technol*. 1971;6:189–193.
33. Rees AC, Davidson JF, Dennis JS, Fennell PS, Gladden LF, Hayhurst AN, Mantle MD, Müller CR, Sederman AJ. The nature of the flow just above the perforated plate distributor of a gas-fluidised bed, as imaged using magnetic resonance. *Chem Eng Sci*. 2006;61: 6002–6015.
34. Müller CR, Holland DJ, Davidson JF, Dennis JS, Gladden LF, Hayhurst AN, Mantle MD, Sederman AJ. Geometrical and hydrodynamical study of gas jets in packed and fluidized beds using magnetic resonance. *Can J Chem Eng*. 2009;87:517–525.
35. Ruzicka M, Drahos J, Zahradnik J, Thomas NH. Natural modes of multi-orifice bubbling from a common plenum. *Chem Eng Sci*. 1999;54:5223–5229.
36. Xiao S, Tan RBH. Bubble formation at multiple orifices-bubble synchronicity and frequency. *Chem Eng Sci*. 2003;60:179–186.
37. Zhang R, Tan RBH. A model for hubble formation and weeping at a submerged orifice. *Chem Eng Sci*. 2000;55:6243–6250.
38. Svensson A, Johnsson F, Leckner B. Fluidization regimes in non-slugging fluidized beds: the influence of pressure drop across the air distributor. *Powder Technol*. 1996;86:299–312.
39. Hoffmann AC, Janssen LPBM, Prins J. Particle segregation in fluidized binary mixtures. *Chem Eng Sci*. 1993;48:1583–1592.
40. Briongos JV, Aragón JM, Palancar MC. Phase space structure and multi-resolution analysis of gas solid fluidized beds hydrodynamics. Part II: dynamic analysis. *Chem Eng Sci*. 2007;62:2865–2879.
41. Kendoush AA. The virtual mass of a spherical-cap bubble. *Phys Fluids*. 2003;15:2782–2785.
42. Davidson JF, Clift R, Harrison D. *Fluidization*, 2nd ed, London, U.K.: Academic Press, 1985.
43. Grace JR, Harrison D. The behavior of freely bubbling fluidised beds. *Chem Eng Sci*. 1969;24:497–508.
44. Clift R, Grace JR. Coalescence of bubbles in fluidized beds. *AIChE Symp Ser*. 1971;67:23–33.
45. Lockett MJ, Davidson JF, Harrison D. On the two-phase theory of fluidization. *Chem Eng Sci*. 1967;22:1059–1066.
46. Svensson A, Johnsson F, Leckner B. Bottom bed regimes in a circulating fluidized bed boiler. *Int J Multiphase Flow*. 1996;22:1187–1204.
47. Fraser AM, Swinney LH. Independent coordinates for strange attractors from mutual information. *Phys Rev A*. 1986;33:1134–1140.
48. Broomhead DS, King GP. Qualitative dynamics from experimental data. *Phys D*. 1986;20:217–236.
49. Grassberger P, Procaccia I. Characterization of strange attractors. *Phys Rev Lett*. 1983;50:346–349.
50. Schouten JC, Takens F, van den Bleek CM. Maximum likelihood estimation of the entropy of an attractor. *Phys Rev E*. 1994;49: 126–129.
51. Baskakov P, Tuponov VG, Filippovsky NF. A study of pressure fluctuations in a bubbling fluidized bed. *Powder Technol*. 1986;45: 113–117.
52. Roy R, Davidson JF, Tuponogov VG. The velocity of sound in fluidised beds. *Chem Eng Sci*. 1990;45:3233–3245.
53. Daw CS, y Halow JS. Evaluation and control of fluidization quality through chaotic time series analysis of pressure drop measurements. *AIChE Symp. Ser*. 1993;89:103–122.

Appendix: On Multiorifice Injection Pattern

According to Figure 1, it is clear that the bubble injection pattern has some influence on the bubble structure developed within the bed. Thus, it can be seen that when using injection patterns such as those of Figures 1a, b, which represent an extreme situation, where there are ''inactive'' regions on the distributor plate, wherever the bubble generation is negligible compared with the actives zones, the resulting bubble dynamical structure is strongly influenced by the bubble generation. That fact is enhanced within the proposed approach due to the fact that the *XY* displacement is motivated by the bubble–bubble interaction. However, when the FB system is

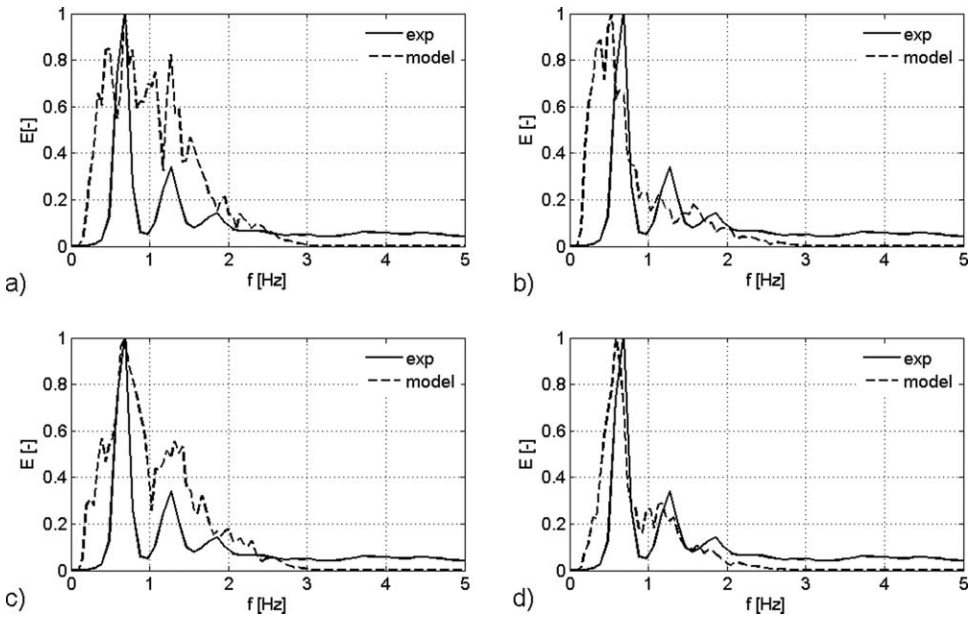

Figure A1. Bubble injection pattern identification, frequency domain analysis.

The simulated time series correspond to the patterns shown in Figure 1, SBR conditions, $N_{or} = 1660$: (a) F1a–p system; (b) F1b–p systems; (c) F1c–p system (uniform); and (d) F1d–p system.

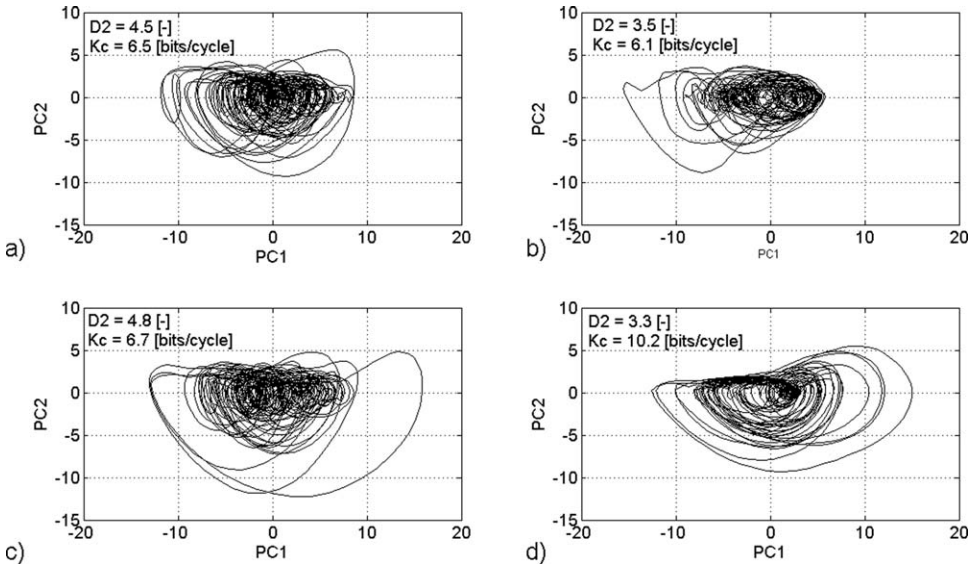

Figure A2. Bubble injection pattern identification, state space analysis. The simulated time series correspond to the patterns shown in Figure 1, F1, SBR conditions, N_{or} = 1660: (a) F1a–p system; (b) F1b–p systems; (c) F1c–p system (uniform); and (d) F1d–p system.

fitted with a uniform gas distributor (Figure 1c), the resulting bubble pattern is not homogeneous and instead of promoting a Type 2 system,[29] the resulting pattern can be identified as a Type 1 system. Accordingly, the pattern is exhibiting preferred paths for rising bubbles and descending solids.

To identify the optimum bubble injection pattern that leads to a dynamical matching between the simulated and measured dynamics, the power spectra of the different bubble generation situations are shown in Figure A1. When comparing the simulated results with the measured pressure time series, Figure A1c that corresponds to a uniform bubble generation pattern is qualitatively and quantitatively very similar to the measured pressure time series. Consequently, the bubble pattern existing within the cold rig under evaluation is identified as a Type 1 system. Once the bubble structure has been identified as Type 1, the bubble generation pattern can be modified facilitating the solid preferred circulation paths (Figure 1d) and improving the matching between the simulated and the measured dynamics (Figure A1d). The state space analysis can be used to help with the injection patter selection (Figure A2). From Figures A1 and A2, it is clear that using different bubble generation patterns is a method for applying the model for dynamical matching purposes.

Manuscript received Oct. 29, 2009, revision received Apr. 28, 2010, and final revision July 8, 2010.